Soils and Foundations 2014;54(4):789–805

The Japanese Geotechnical Society

Soils and Foundations

www.sciencedirect.com
journal homepage: www.elsevier.com/locate/sandf

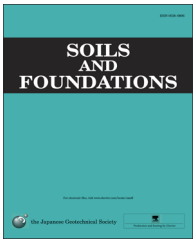

Stability of caisson-type breakwater foundation under tsunami-induced seepage

Hidenori Takahashi[a,*], Shinji Sassa[a], Yoshiyuki Morikawa[a], Daiki Takano[a], Kenji Maruyama[b]

[a]*Port and Airport Research Institute, Yokosuka, Japan*
[b]*Geodesign Corporation, Tokyo, Japan*

Received 8 May 2013; received in revised form 28 March 2014; accepted 21 April 2014
Available online 4 August 2014

Abstract

A tsunami-induced difference between the water levels of the seaward and the landward sides of breakwaters generates one-way seepage in the rubble foundation under the breakwaters. Such seepage may decrease the bearing capacity of the rubble foundation, trigger the piping and/or boiling of the foundation, and cause the scouring of the sandy seabed. In this paper, we describe the stability of a breakwater foundation under the action of seepage based on the results of model tests and FEM analyses. The main feature of our study is the application of the centrifuge technique to such composite hydrodynamic and geotechnical problems. The centrifuge technique can be used to produce high-water pressure and ground stress corresponding to those of prototype-scale breakwaters. The experimental results show that seepage-induced scouring and boiling occur, and that the seepage force decreases the bearing capacity of the rubble foundation. The results of the numerical analyses also reveal the effect of the reduction in bearing capacity in the presence of seepage.

Keywords: Breakwater; Tsunami; Seepage; Bearing capacity; Boiling; Centrifuge model test; Finite element method (IGC: E-7/E-14)

1. Introduction

Several forces, such as those shown in Fig. 1(a), can act on both the caisson and the foundation of a breakwater when it is subjected to a tsunami. If the foundation, which includes a rubble foundation and the seabed, is sufficiently strong, a strong wave force would trigger the sliding and/or the overturning of the caisson. However, if the strength of the foundation is insufficient, other failures may occur in the foundation, as shown in Fig. 1(b), such as failure by an inclined load applied by the caisson, the scouring of the rubble foundation by the overflow water force, piping or boiling by the seepage force, and scouring of the seabed. It should also be noted that these failures may occur simultaneously in some cases.

Tsunamis generate a long-duration difference between the water levels of the seaward and the landward sides of breakwaters, which is different from that generated by the waves produced by strong winds. This difference in water levels generates seepage flow and force in the rubble foundation and may reduce the bearing capacity and cause scouring of the seabed, as well as piping and boiling of the rubble foundation. This is because the difference in water levels produces an upward force and decreases the confined pressure, the stiffness, and the strength of the rubble foundation. The seepage simultaneously generates a horizontal force in the direction

*Corresponding author.
E-mail address: takahashi-h@pari.go.jp (H. Takahashi).
Peer review under responsibility of The Japanese Geotechnical Society.

http://dx.doi.org/10.1016/j.sandf.2014.07.002
0038-0806/

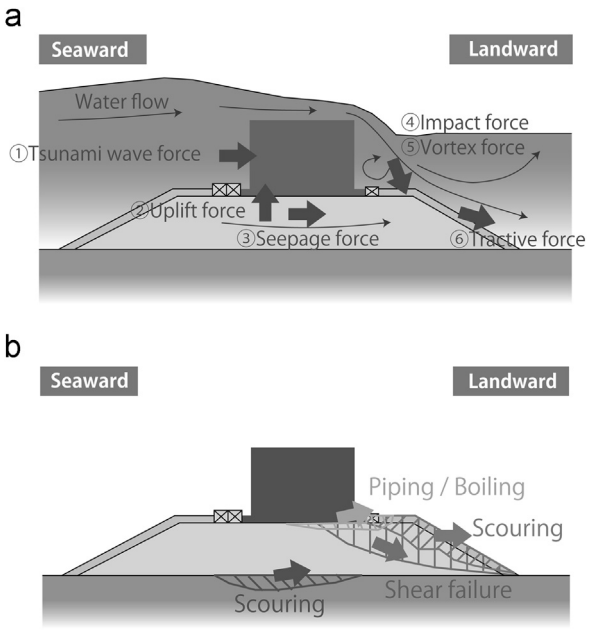

Fig. 1. Forces on breakwaters and their failures. (a) Forces, (b) failure modes.

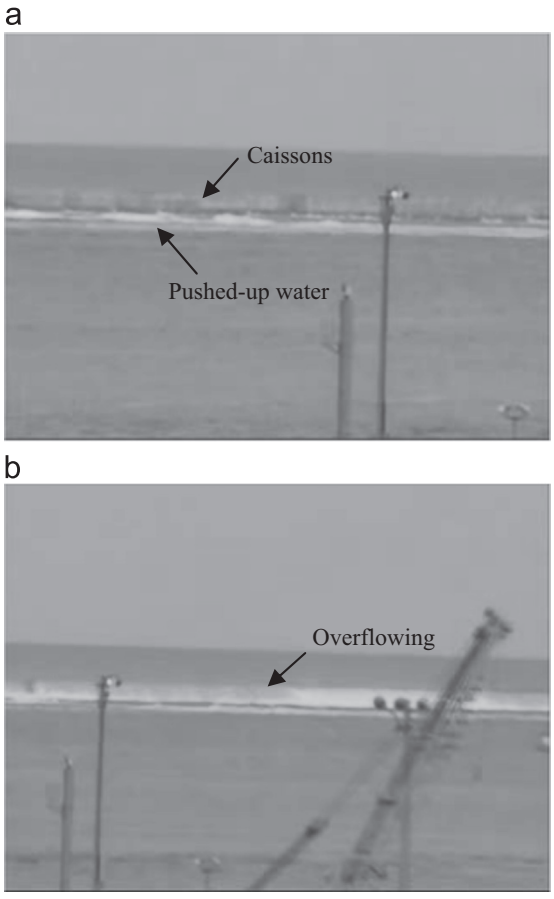

Fig. 2. Kamaishi breakwaters (a) before and (b) after overflowing.

of the embankment toe. It is important, therefore, to take into consideration the seepage in a rubble foundation when assessing the stability of the foundation in the event of a tsunami.

The damage to breakwaters caused by the massive tsunami that followed the Great East Japan Earthquake on 11 March 2011 (Kazama and Noda, 2012) highlighted the importance of considering the instability of a foundation under seepage. During this tsunami, many breakwaters were displaced from rubble foundations and some foundations even collapsed. Although details of the breakwater failure mechanism have not been clarified, because of the severe damage, no doubt the seepage force affected the stability of the rubble foundations. Fig. 2 shows pictures of the Kamaishi north breakwaters (length 990 m) when they were hit by the tsunami. The two pictures were captured 17 min and 19 min after starting the video filmed by the Ministry of Transport of Japan. The water that was pushed up by the seepage flow can be seen behind the breakwaters in the picture before the overflow. This reveals that there was a very strong seepage flow through the rubble foundation. Before the tsunami, critical factors for breakwater designs in Japan had mostly dealt with the strong wave forces generated by a typhoon or atmospheric depression. Since the tsunami, however, the predicted tsunami heights used for the design of most breakwaters have been raised, and the ability to cope with tsunamis has become a critical factor of many breakwaters. This has led to giving due consideration to the effect of seepage at the design stage.

Several studies have been conducted on the stability of rubble-mound and submerged breakwaters under the attack of a tsunami (Fujima, 2006; Ergin and Balas, 2006; Lin and Karunarathna, 2007; Irtem et al., 2011), and on the various design procedures applied to them (ICE, 1994; PIANC, 2003). However, few studies have been done globally on the stability of caisson-type breakwater foundations under seepage induced by a tsunami. In Japan, Imase et al. (2011, 2012) introduced drum-type centrifuge tests and numerical analyses using the smoothed-particle hydrodynamics (SPH) method to examine the instability of a breakwater foundation subjected to a tsunami. In their study, the tsunami, which was produced by a dam-break method, was made to hit the breakwater in a centrifuge. However, the specific effect of seepage on the stability of a breakwater foundation could not be clarified, because many types of forces, such as wave, uplift, and seepage forces, simultaneously act on a breakwater. Ikari et al. (2011) also demonstrated a new numerical investigation of the instability of a breakwater foundation by the MPS method. They used the elasto-plastic model and Darcy's law to study the solid and liquid behaviours, and also solved the equations that couple the soil particles and the pore water. These numerical methods are to be further developed in the future. Dong et al. (2012), Chen et al. (2013), and Zen et al. (2013) demonstrated both the pop-out failure of armoured blocks and the reduction in bearing capacity due to tsunami-induced seepage using model tests in the gravitational field and some numerical analysis techniques. These studies showed the possibility of the pop-out failure of blocks and the reduction in bearing capacity due to seepage force. However, the bearing capacity was assessed based on the amount of settlement of a caisson, and not the ground strength related to the bearing

capacity. Moreover, it was not possible to distinguish between the effects of seepage and uplift forces on the bearing capacity.

These previous studies were insufficient for understanding the specific effect of seepage on the foundation of a breakwater. Therefore, the aim of the present study is to describe the stability and the bearing capacity of a breakwater foundation under seepage using centrifuge model tests and finite element analyses. The main feature of this study is the application of a centrifuge technique to such composite hydrodynamic and geotechnical problems. A centrifuge can be used to produce both high-water pressure and ground stress corresponding to prototype-scale breakwaters.

Since the 1960s, centrifuge techniques have been used to solve various geotechnical problems owing to the high stress corresponding to a prototype scale that is needed to simulate non-linear ground behaviour. In contrast, hydrologic tests have been conducted in a gravitational field. This is because there are clear and proven equations that govern the behaviour of fluids, such as Froude's and Reynolds' laws. Against this background, several hydraulic and geotechnical problems have recently been revealed. Sekiguchi et al. (1995) and Sassa and Sekiguchi (1999) first used a centrifuge technique to observe the behaviour of grounds subjected to wind waves. Miyake et al. (2009) conducted a number of experiments on the impact of waves on port facilities using a drum-type centrifuge machine with a long water channel. Takahashi et al. (2010) also used a centrifuge to simulate ground behaviour in a wave breaker zone. In addition, Bezuijen and Steedman (2010) and Beek et al. (2010) summarized hydraulic experiments conducted in a centrifuge and demonstrated piping in a river embankment. Wang et al. (2010) used a new circulating system for water supplies to investigate the stability of an embankment against overtopping water. Further centrifuge tests on composite hydrodynamic and geotechnical problems will be conducted in the future.

In the present model tests, in which a centrifuge was used, the seepage in a rubble foundation was produced by generating a difference between the water levels of the seaward and the landward sides of the breakwaters. The rubble foundation was then observed to determine whether piping and/or boiling had occurred in it under seepage. Moreover, the bearing capacity under seepage was assessed. To examine the more detailed characteristics of the bearing capacity, numerical analyses were conducted using a finite element method. To focus on only the failures caused by seepage, the effect of foundation scouring by the overflow water was excluded from the present study. In addition, in the appendices at the end of this paper, we discuss the similarity rule and the applicability of a centrifuge technique to seepage in rubble rocks. To the best of the authors' knowledge, there has been no previous study to demonstrate this applicability, and therefore, some model tests were conducted to verify it.

2. Experimental system for simulating seepage in centrifuge

The beam-type centrifuge machine, owned by the Port and Airport Research Institute of Japan (Kitazume and Miyajima, 1995), was used for the model tests (see Fig. 3(a)).

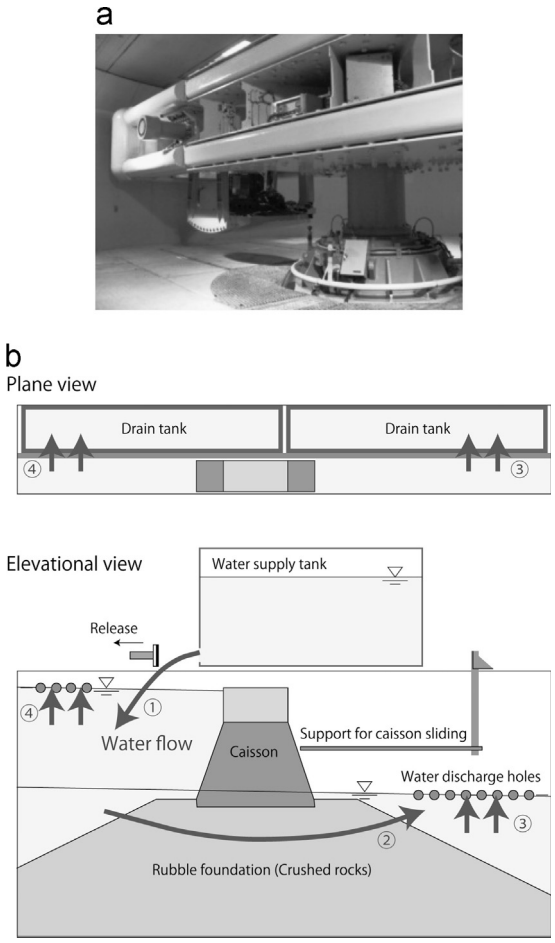

Fig. 3. Centrifuge and seepage system. (a) Geotechnical centrifuge PARI Mark II, (b) dam-break method as seepage system.

It includes a large square platform measuring $1.6 \times 1.6\ m^2$, which can hold a large specimen container with an inner length as long as 1.2 m. The centrifuge can be used to simulate the behaviour of a 60-m-long ground by setting the centrifugal acceleration to 50*g*.

A pump that can produce continuous water flow is ideally used to model the seepage flow system. However, the modelling requires large amounts of water, and the pumping head in a centrifuge is significantly large. These factors mean that a fair-sized pump is required for the tests. However, the use of a pump in the centrifuge was not possible in this case due to the restrictions of both power supply and space. Therefore, a dam-break method was adopted in the present experiment, as shown in Fig. 3(b), wherein water was held in a water supply tank and then suddenly released. Here, the horizontal flow of a tsunami was not reproduced in the model tests. This is because flow energy is generally converted to potential energy at the front of the breakwaters, and the water level difference included this flow energy.

It is known that the dam-break method cannot be easily used to control either the flow volume or the water level. However, in the present model tests, the water level could be controlled by discharging excess water through holes created in the back

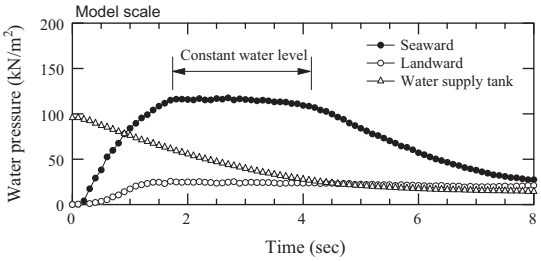

Fig. 4. Example of time histories of excess water pressure of the seaward and landward.

wall. The water discharged through the holes was collected in two tanks set up behind the wall. Samples of the excess water pressure, measured seaward and landward, are shown in Fig. 4, which includes the water pressure measured at the bottom of the water supply tank. The measured pressure was then converted to corresponding values for the prototype scale. In can be seen from the figure that the pressure of the seaward and the landward breakwaters rose for about 1.7 s and then remained constant for 2.5 s. This period corresponds to 125 s on the prototype scale, which sufficiently simulates the duration of a local or near-field tsunami.

The centrifuge machine was stopped after a test run, and the model ground was thereafter repaired and/or prepared in the gravitational field. The water in the drain tanks was then pumped up to the water supply tank. The seepage flow tests conducted in the centrifuge were repeated for different model ground conditions.

After the model tests, the ground deformation was determined by the digital image correlation (DIC) technique. DIC is a mathematical tool for assessing the spatial transformation between images. The 2D-DIC analysis code used in this paper was developed by referencing (Hall, 2006). The code follows the same basic steps of most DIC procedures for strain analyses.

3. Stability of breakwater foundation under seepage

3.1. Materials and test cases

Fig. 5 is a schematic of the experimental profiles used to examine the possibility of the scouring of the seabed and the piping and/or the boiling of the rubble foundation by the seepage produced by a tsunami. One of the profiles models the Kamaishi breakwaters in Japan for a dimensional ratio of 1/112.5. The dimensional ratio of the prototype scale for a centrifugal acceleration of 75g is 1/1.5. Another one of the profiles models the Omaezaki breakwaters in Japan. Here, the dimensional ratios are 1/50 and 1/1 for the model and the prototype scales, respectively. The test for which the Omaezaki model was applied was conducted using a centrifugal acceleration of 50g. The other tests were conducted using a model produced by reducing the width and the height of a caisson of the Omaezaki model, which is referred to as the deformed Omaezaki model in this paper. The width was shortened as a way to increase the hydraulic gradient in the rubble foundation.

All the cases are listed in Table 1. Two types of rubble stones were used, namely, Rock A and Rock B (see Fig. 6). The similarity rule and the applicability of the centrifuge technique to the seepage force in the rubble rocks are discussed in the appendices at the end of this paper. Rock A comprised a 1:1 mixture of crushed stones and Sohma silica sand cat. 2 (excavated from Fukushima Prefecture, Japan). The crushed stones had an average particle size of 5 mm and a weight of 0.17 g, which corresponded to 71.7 kg under a centrifugal acceleration of 75g. The average particle size and weight of the Sohma silica sand were, respectively, 2 mm and 0.013 g, which corresponded to 5.5 kg. The weights ranged from 0.011 to 0.58 g, and the wet and dry unit weights were, respectively, 19.9 and 16.5 kN/m^3. Rock B also consisted of crushed stones with an average particle size of 10 mm and a weight of 1.26 g, which corresponded to 157.5 kg under a centrifugal acceleration of 50g. The weights ranged from 0.50 to 3.51 g, and the wet and dry unit weights were, respectively, 19.6 and 15.7 kN/m^3. The sand used for the seabed was Sohma silica sand cat. 5. The average particle size of the sand was 0.36 mm.

The centrifugal acceleration was 50g, except for Case KM04 of the Kamaishi model, for which the centrifugal acceleration was 75g. Table 1 includes the differences between the water pressure levels of the seaward and the landward breakwaters. In the tests with the deformed Omaezaki model, the water level difference was varied to assess its effect on the piping or the boiling of the rubble foundation. The positions of the caissons were maintained in all the tests in order to distinguish the foundation failure from the movement of a caisson.

3.2. Test results on scouring of seabed

Fig. 7 shows successive pictures of the seabed for Case OM01 taken at intervals of 0.33 s. It can be observed that the seabed was continuously scoured below the front bottom corner of a caisson, although the amount of scouring is not discussed here due to the insufficient verification of the sand scouring in the centrifuge. Some of the scoured sand piled up in the void of the foundation and beyond the foundation. The particle size of the Sohma silica sand was much smaller than that of the crushed stones. Therefore, the surface of the seabed was partially exposed to seepage flow in the void of the foundation and was gradually scoured. The sand that piled up in the void of the foundation hindered the seepage flow, thereby causing concentration of the seepage force in that area.

The scouring of the seabed was also seen to have caused the settlement of a caisson, the rubble foundation, and large crushed stones in front of the caisson. Members of the breakwaters, subjected to repetitive leading waves and backwash, such as a caisson, were expected to settle as a result of the scouring of the seabed. The settlement of a caisson may reduce the bearing capacity, due to the increase in buoyancy, which in turn decreases the confining pressure and the shear strength of the rubble foundation.

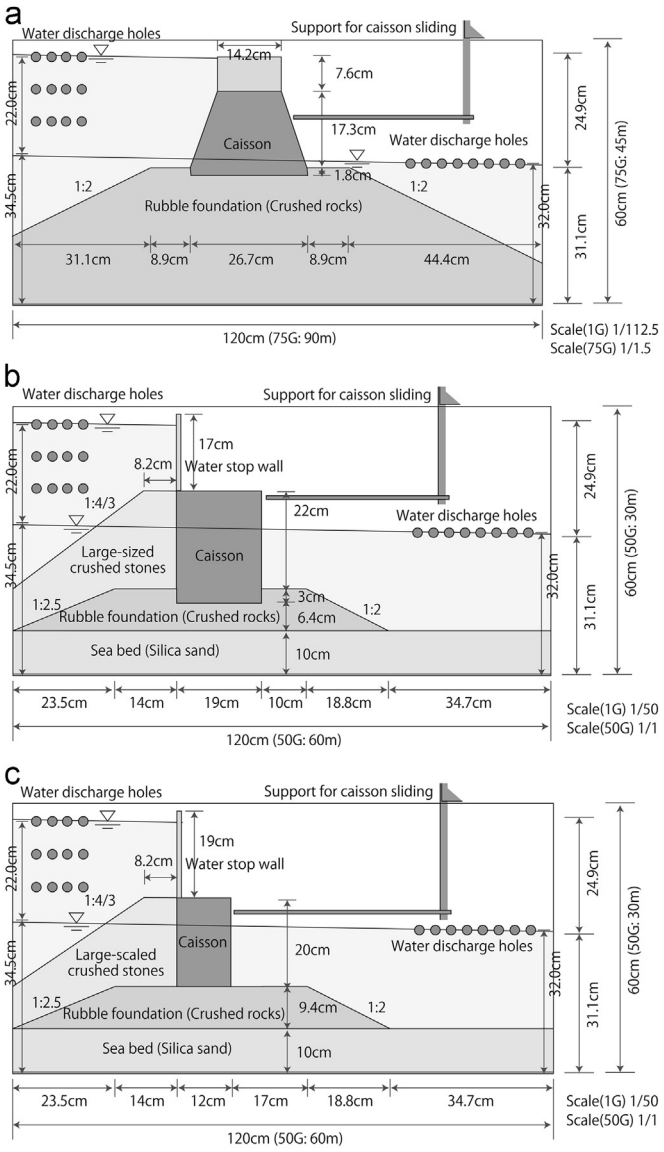

Fig. 5. Schematic views of breakwaters model for observation of scouring, piping and boiling. (a) Kamaishi model, (b) Omaezaki model, (c) deformed Omaezaki model.

3.3. Test results on piping and boiling of rubble foundation

3.3.1. Characteristics of excess pore water pressure

Fig. 8 shows the excess pore water pressure under seepage for three representative cases, measured immediately after the water level difference became steady. For Case OM08, spatially averaged hydraulic gradient i remained low at 0.4 for a water pressure difference of 81 kN/m^2. Moreover, the large crushed stones, which were used to model wave-dissipating blocks, somewhat disturbed the water flow and produced an asymmetric distribution of excess pore water pressure. For Cases KM04 and OMD05, the spatially averaged values for i under the caissons were 0.6 and 1.1, respectively. These two gradients were higher than that of Case OM08.

According to theory, boiling occurs in a non-loaded ground when seepage force $i\gamma_w$ becomes equal to effective unit weight γ'. Fujikura and Kokusho (2001) conducted element tests for various types of sand and gravel, and demonstrated the relationship between the hydraulic gradient and seepage failure, including piping and boiling. Several remarkable results, related to the present study, can be found in their work. For example, specimens with a uniformity coefficient U_c of below 4 did not split off under low i. In addition, they almost boiled when subjected to the theoretical limit hydraulic gradient i_c. Furthermore, the U_c of the specimen, which was nearly 1.0, had little effect on the hydraulic gradient that triggered the seepage failure. Chang and Zhang (2013) also summarized similar results.

Based on the above results, boiling would theoretically occur for the i_c of the present model tests because U_c was close to 1.0. Since the effective unit weights of Rock A and Rock B were, respectively, 9.9 and 9.6 kN/m^2, the i_c values in the non-loaded ground were, respectively, 1.01 and 0.98. Only for Cases OMD02 and OMD05 had i been expected to exceed these i_c values, indicating the possibility of piping and/or boiling.

3.3.2. Observation of piping and boiling of rubble foundation

No piping was observed in any of the model test results. However, some rocks on the ground around the corner of the caisson had turned over in Cases OMD02 and OMD05 for high values of hydraulic gradient i. This behaviour was considered as light and insignificant boiling. The successive pictures in Fig. 9(a) show rolling rocks, whereas Fig. 9(b) shows traces of the light boiling that occurred in Case OMD05. The boiling in this case, where i exceeded the limit value, indicated that the seepage failures occurred in accordance with theory. In addition, the present experiments, in which prototype-scale stress was generated, revealed that no significant piping or boiling was produced by the seepage force itself. The non-occurrence of significant piping or boiling was confirmed by observation of the real field of the Kamaishi breakwaters. Fig. 10 shows a sample sounding-map of the rubble foundation beside the caissons that remained after the tsunami. It was reported that there was no trace of piping or boiling in any of the foundations that remained, including the ones shown in the figure.

There are three possible explanations for why neither piping nor boiling significantly developed. One is the effect of loading from the upper caisson. The foundation loaded by the caisson had a relatively high confined pressure and resistive force against piping and boiling. Another is the awkward shape of the foundation rocks. When the foundation rocks move with the seepage force, it is possible that their shapes will cause them to become lodged. The third explanation, which is similar to the second one, is the localization of the soil. Soil localization tended not to occur in the crushed stones compared to the fine sand, which prevented piping.

These explanations also suggest that adequate loading from a caisson and the absence of small particles in the rubble foundation were key factors in preventing piping and boiling in the test foundations. Furthermore, increasing the width of a caisson or embedding one in the rubble foundation obviously affects the stability by reducing i.

Table 1
List of test cases for observation of scouring, piping and boiling.

Case	Profile	Rock used	Centrifugal acceleration (g)	Water pressure difference (kN/m^2)
(a) Observation of scouring of foundation				
OM01	Omaezaki	B	50	74
(b) Observation of piping and boiling				
OM08	Omaezaki	B	50	81
KM04	Kamaishi	A	75	165
OMD01	Deformed Omaezaki	B	50	83
OMD02				110
OMD03		A		54
OMD04				90
OMD05				116

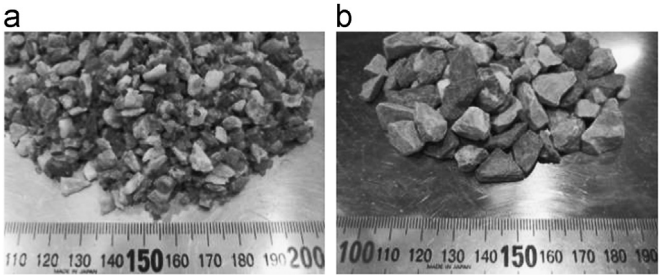

Fig. 6. Rubble stones used for tests. (a) Rock A and (b) Rock B.

4. Bearing capacity characteristics determined by model tests

4.1. Test cases and materials

A decline in bearing capacity may occur as a result of two factors, namely, a decrease in the confined pressure owing to an uplift force acting on a caisson, and the seepage force acting on the rubble foundation. The former is not a difficult problem and can be easily taken into account in breakwater designs, whereas the latter is more difficult and its effect has yet to be clarified. Therefore, the aim of the present study is to examine the effect of the latter problem.

Four profile types were used to examine the decrease in bearing capacity, namely, the profile of the horizontal loading tests without seepage, and the profiles of the tests in which horizontal loading was combined with seepage. These profiles were produced virtually and three of them are shown in Fig. 11. As shown in the figure, the applied foundation had a high slope top and gradient and a narrow slope top. These features were selected to dominate the ground failure rather than the movement of a caisson. The profile omitted from the figure was similar to virtual model A and had a 40-mm counterweight fill (corresponding to 2 m on the prototype scale), which was used to increase the bearing capacity.

The seepage was generated after loading a caisson with weights using a pulley and wire, as shown in Fig. 11(b) and (c). This procedure was used because the seepage period was not sufficiently long to load the caisson by a motor jack during seepage. The seepage test profiles also had a water stop wall that caused seepage from the bottom. The wall created no water level difference between the two sides of the caisson and could eliminate the uplift force acting on the caisson. Furthermore, the permeability of the caisson was enhanced by drainage holes, which prevented the accumulated water pressure from lifting the caisson. It must be noted that the seepage flow from the bottom could cause a greater reduction in the bearing capacity than the lateral flow.

The test cases are listed in Table 2. The applied crushed stones were the previously used Rock A and Rock B, and the centrifugal acceleration was set to 50g. The water pressure difference was 115 kN/m^2. In Cases BC01 and BC12, the rubble foundations were demolished by the horizontal loading by a motor jack without seepage. In Cases BC02–BC05 and BC06–BC11, the deformation of the rubble foundations was observed under both loading and seepage.

4.2. Results of horizontal loading tests

Fig. 12 shows the relationship between the load and the displacement for Cases BC01 and BC12 on the prototype scale. The displacement was measured from 50 mm below the top of the caisson. The load and the displacement were measured using a cantilever-type load cell and a displacement gauge, respectively. As a rubble foundation exhibits relaxation behaviour, the caisson was intermittently loaded.

The relationship between the load and the displacement was initially non-linear, which indicated plastic deformation. After a

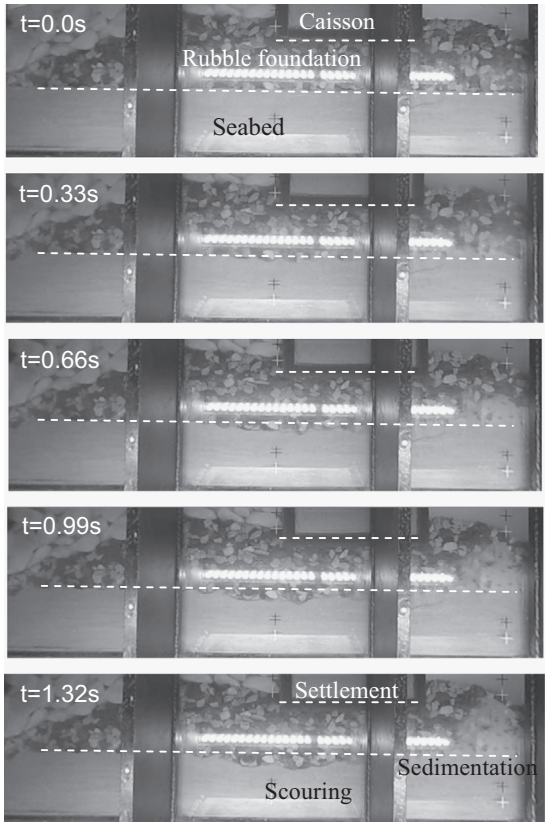

Fig. 7. Successive pictures taken in Case OM01.

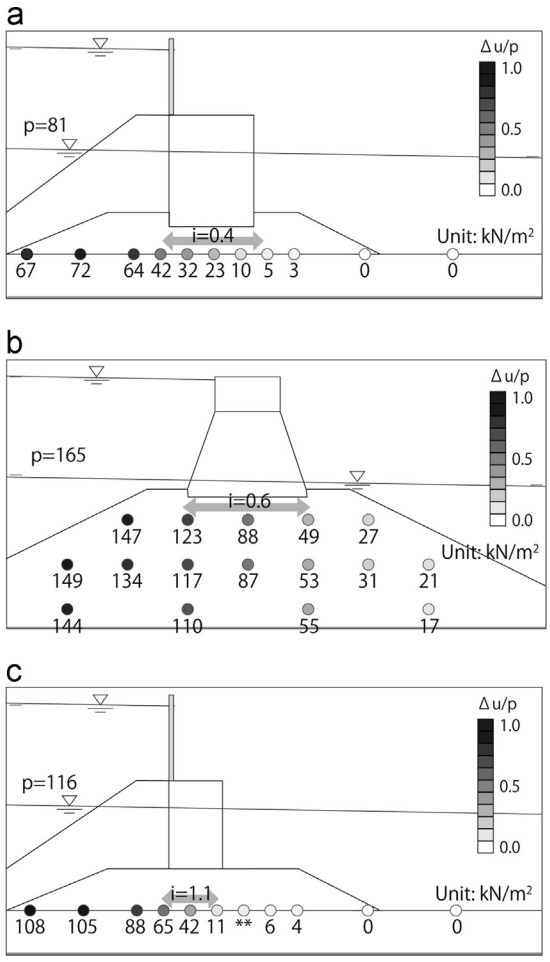

Fig. 8. Distributions of excess pore water pressure in (a) Cases OM08 (Omaezaki), (b) KM04 (Kamaishi), (c) OMD05 (Deformed Omaezaki).

displacement of 0.6 m, the relationship became almost linear, and the starting point of the straight line was considered to be the beginning of the limit state of the ground. The horizontal loads at these points for Cases BC01 and BC12 were 815 and 861 kN/m, respectively. In the seepage tests mentioned below, the seepage was generated under horizontal loads that were less than the foregoing loads. In addition, it was confirmed that the foundation failure occurred before the sliding and overturning of the caisson, which theoretically occurred at loads of about 1050–1250 and 1090 kN/m, respectively. The load that caused sliding can be calculated by multiplying the weight of the caisson by the coefficient of friction, μ, which was 0.57–0.68, as obtained by a friction test. The load that caused overturning can also be calculated by dividing the moment produced by the weight of the caisson by the height of the loading point. Although these loads contain some errors, it was found that the load that caused the foundation failure was much lower than those that caused the sliding and the overturning of the caisson.

Fig. 13 shows the deformed area and the magnitude of the deformation in the rubble foundation of Case BC12, where the amount of deformation is indicated by contrasting shades. These were obtained by the DIC technique. The two diagrams in Fig. 13 show the accumulated deformation before and after the beginning of the limit state, respectively. As shown in Fig. 13(a), the large and deep area in the rubble foundation was deformed before the limit state. However, as shown in Fig. 13(b), the deformed area was concentrated at both the corner of the caisson and the top of the slope in the limit state, and the magnitude was large. This transition means that the strain induced by the loading was concentrated as a result of the strain localization in the rubble foundation.

Fig. 14 shows the displacement vectors, which were also determined by the DIC technique. The two figures show the vectors for Cases BC01 and BC12, respectively, up to a caisson displacement of 1.5 m. In both figures, there is a laterally and downward deformed area under the corner of the caisson, which caused the top of the slope to move forward. The behaviour observed here is a typical failure mode caused by inclined loading, and higher shear strength under the caisson and a counter weight placed on top of the slope can be used to increase the bearing capacity.

4.3. Results of tests combining horizontal loading and seepage flow

4.3.1. Characteristics of excess pore water pressure

The excess pore water pressure shown in Fig. 15 was measured at different points for Cases BC02 and BC06 immediately after the difference in water levels became steady. In Case BC02, the excess pore water pressure under the water stop wall was low. This is a situation in which, according to

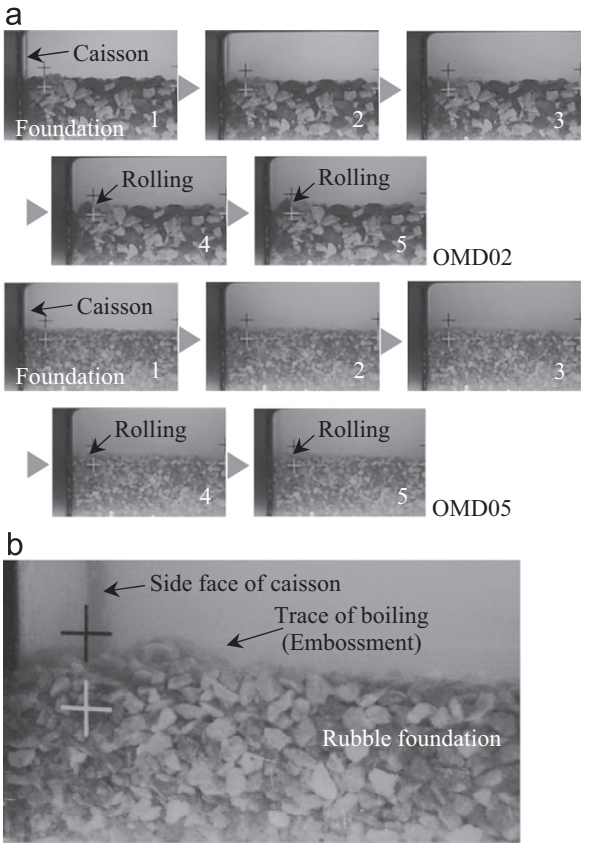

Fig. 9. Rolling rocks and light boiling by seepage, (a) rolling rocks in OMD02 and OMD05, (b) trace of light boiling in OMD05.

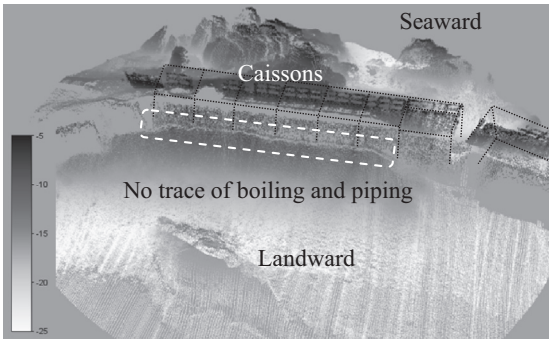

Fig. 10. Sounding-map of rubble foundation after tsunami.

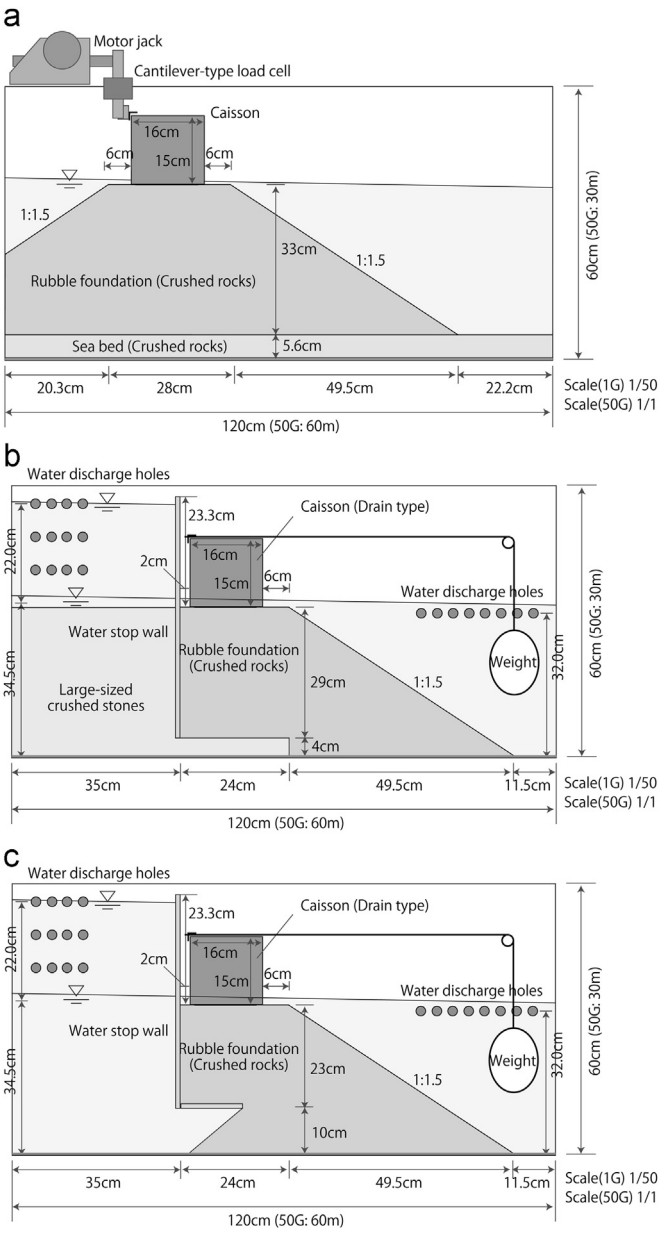

Fig. 11. Schematic views of breakwaters model for verification of bearing capacity reduction, (a) horizontal loading test model, (b) virtual model B (Rock B), (c) virtual model A (Rock A).

theory, hydraulic gradient i in the rubble foundation would remain low. Although i was not directly measured in this case, it could be determined by the above-mentioned numerical analyses, which produced a value of about 0.1 around the top of the slope. This value was low.

In Case BC06, the amount of water supplied to the rubble foundation was increased by widening the outlet under the water stop wall, and large crushed stones were not placed in front of the wall. These changes were made to allow a significant amount of water to percolate into the rubble foundation. Fig. 15(b) shows the excess pore water pressure for Case BC06. It can be seen that the water pressure under the wall was not reduced from 115 kN/m^2, and that i around the top of the slope reached 0.4.

4.3.2. Reduction in bearing capacity

Fig. 16 shows the results for the cases in which the seepage was synchronized with the horizontal loading, and the results of the horizontal loading tests shown in Fig. 12. Each figure shows the data for Cases BC02–BC05 (virtual model B) and BC06–BC11 (virtual model A) on the prototype scale, respectively. The filled and open circles represent the displacements before and after seepage, respectively.

As shown in Fig. 16(a), all the caissons were displaced by the seepage force. There was particularly significant displacement in Case BC05. The movements of the caissons indicated

Table 2
List of test cases for verification of bearing capacity reduction.

Case	Profile	Rock used	Horizontal load (kN/m)*	Remarks
BC01	Horizontal loading	B	Gradual increase	Loading
BC02	Virtual model B		319	Loading+ Seepage
BC03			433	
BC04			548	
BC05			663	
BC12	Horizontal loading	A	Gradual increase	Loading
BC06	Virtual model A		319	Loading+seepage
BC07			433	
BC10			548	
BC08			663	
BC11	Counter embankment model		663	

* Loads are represented in a prototype scale.

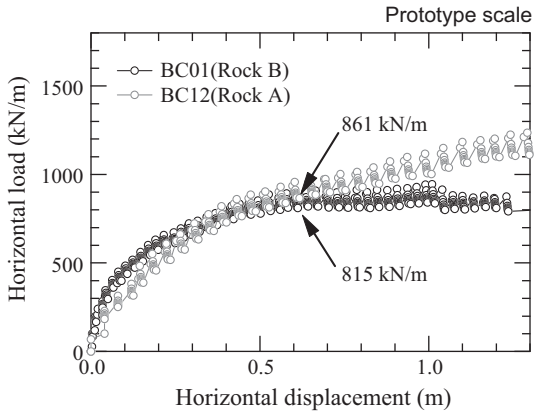

Fig. 12. Relationship between load and displacement in Cases BC01 and BC12.

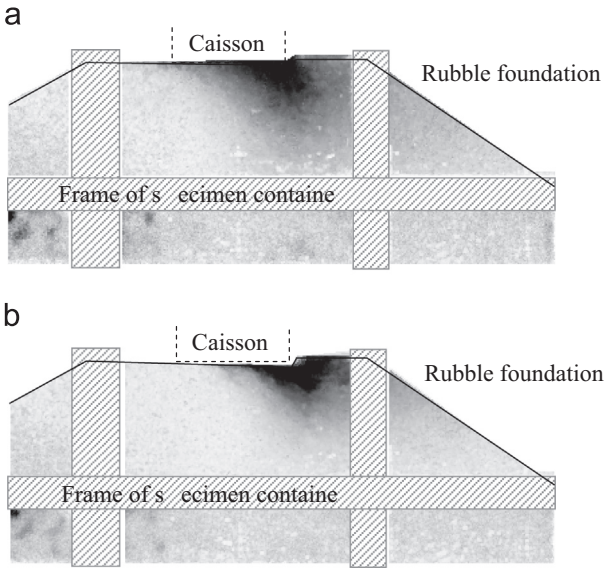

Fig. 13. Deformed area and its degree in Case BC12, (a) before beginning of limit state, (b) after beginning of limit state.

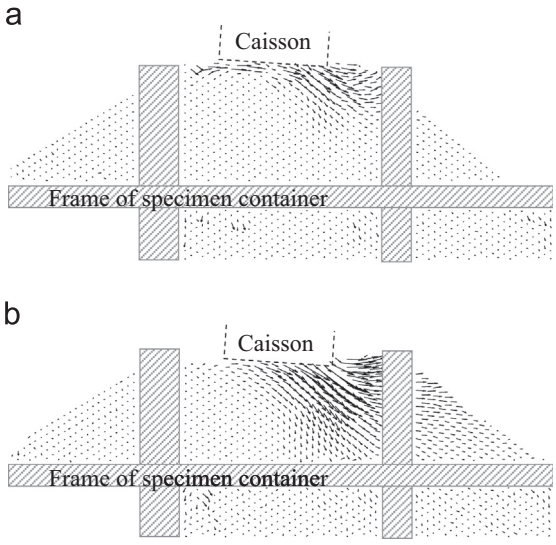

Fig. 14. Displacement vectors in Cases (a) BC01 and (b) BC12.

a reduction in the bearing capacity due to the seepage. Fig. 16 (b) shows that the displacements in Cases BC06–BC11, in which higher hydraulic gradients were generated, were larger than those in Cases BC02–BC05. In Case BC08, which was characterized by both substantial seepage and a large horizontal load, devastating ground failure occurred and the caisson fell from the foundation.

Fig. 17 shows successive pictures that capture the moment of the foundation failure and the displacement vectors calculated by the DIC technique. Regarding Fig. 17(a), it had first been confirmed by the model tests that the seepage force itself could break down the rubble foundation under an inclined load. The deformation behaviour shown in Fig. 17(b) was quite similar to that in Fig. 14, which was obtained by the horizontal loading test, and it shows that the mechanisms of the foundation collapse were the same.

The horizontal loads in Cases BC10 and BC08 were 548 and 663 kN/m, respectively. The bearing capacity of the rubble foundation under seepage must be between the two values

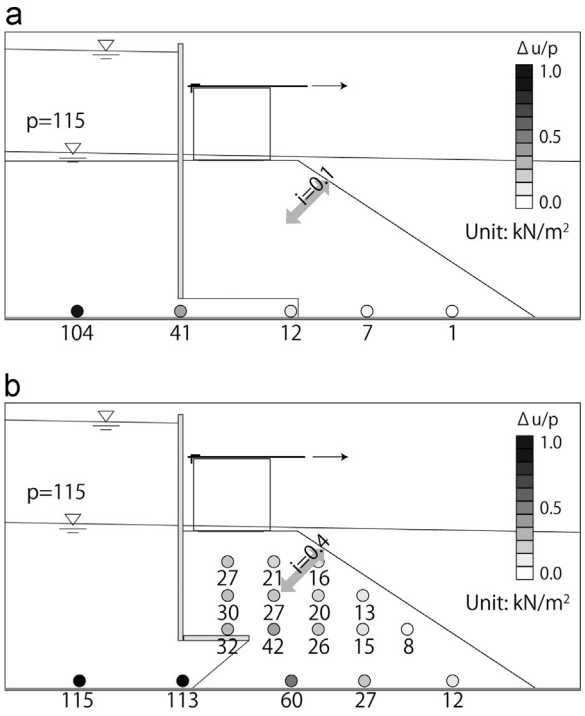

Fig. 15. Distributions of excess pore water pressure in Cases (a) BC02 and (b) BC06.

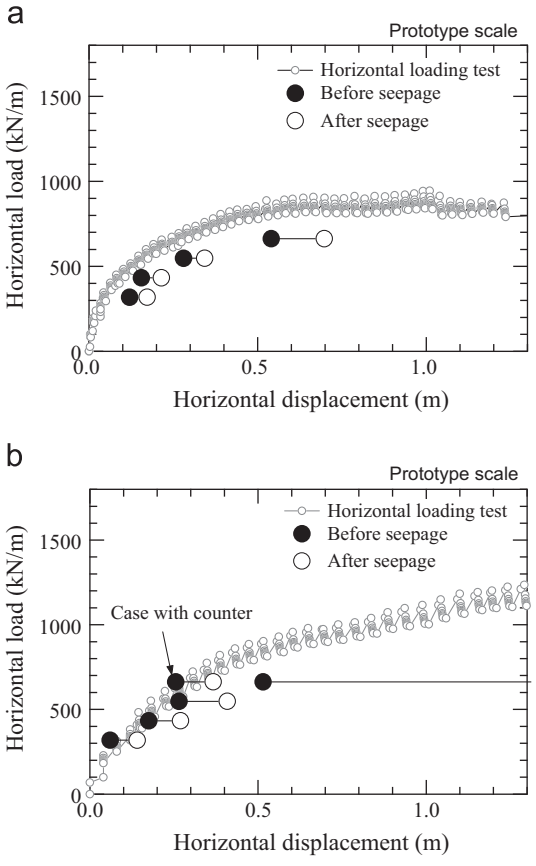

Fig. 16. Relationship between load and displacement in Cases (a) BC02–BC05 (Virtual model B) and (b) BC06–BC11 (Virtual model A).

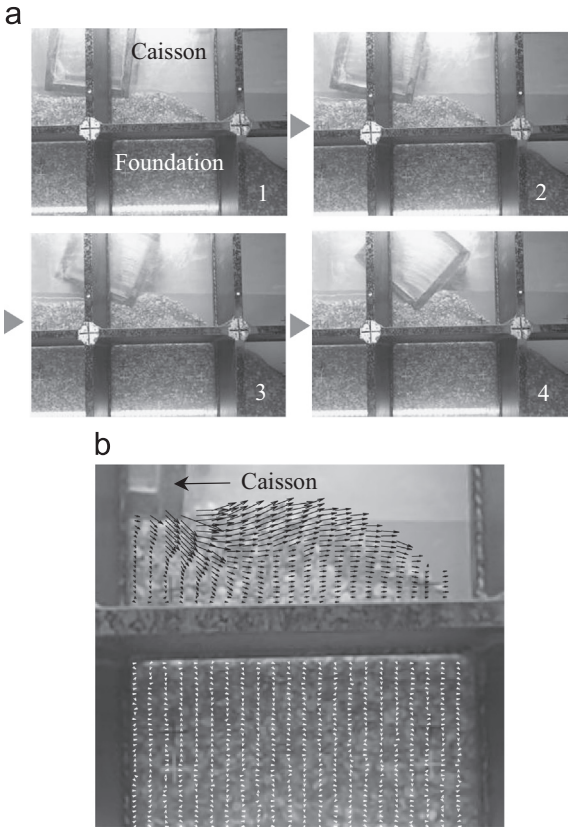

Fig. 17. Successive pictures and displacement vectors in Case BC08, (a) successive pictures of foundation failure, (b) displacement vectors.

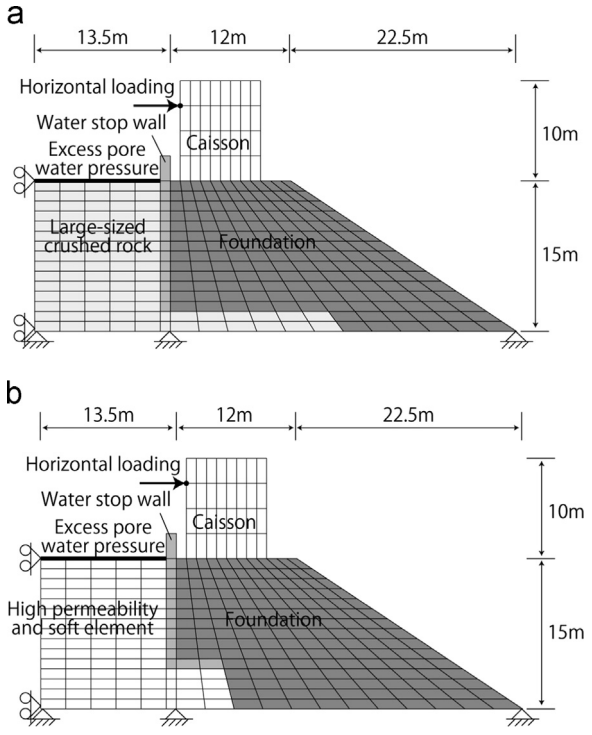

Fig. 18. Finite element mesh modelling virtual models A and B. (a) Virtual model B, (b) Virtual model A.

Table 3
Parameters for numerical analyses.

	E (MN/m^2)	γ' (kN/m^3)	c (kN/m^2)	ϕ (°)	k (m/s)
Rubble Foundation	29.4	9.8	20	35	0.2
			0	45	
Caisson/water stop wall	196.0	22.8	–	–	–
Crushed stone	29.4	9.8	–	–	0.28

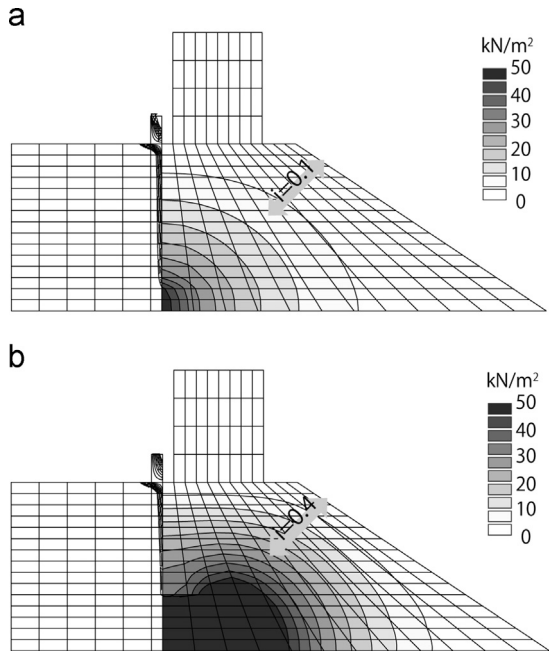

Fig. 19. Distribution of excess pore water pressure in virtual models A and B. (a) Virtual model B, (b) Virtual model A.

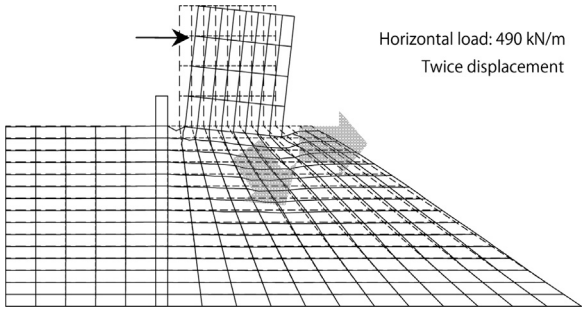

Fig. 20. Deformation behaviour of virtual model A.

because the foundation of Case BC10 did not collapse, whereas that of Case BC08 collapsed. However, Fig. 12 shows that the bearing capacity without seepage was 861 kN/m based on the load at the beginning of the limit state. This means that the bearing capacity was decreased by the seepage force to 64–77%. The reduction is 23–36%, which is larger than the reduction observed in commonly used breakwaters due to the above-mentioned seepage from the bottom.

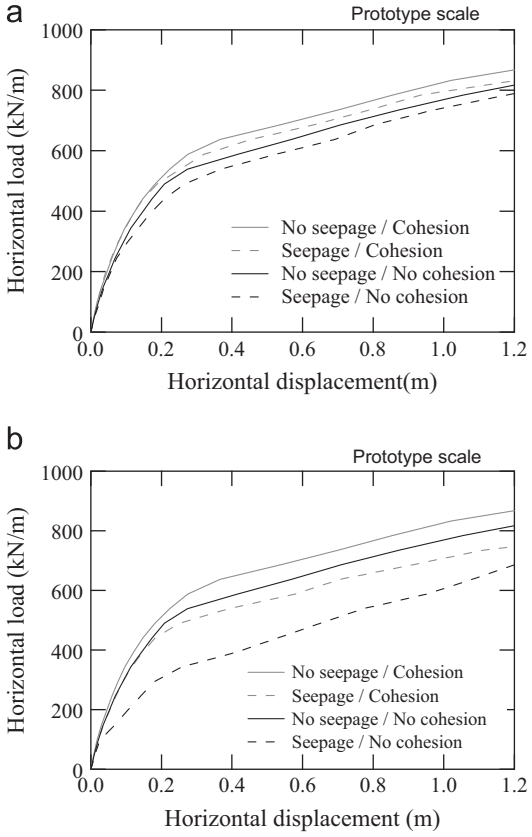

Fig. 21. Relationship between load and displacement at the top of caisson, (a) virtual model B, (b) virtual model A.

In Case BC11, which had the same horizontal load as Case BC08, no failure was observed, and the counterweight fill affected the bearing capacity.

5. Bearing capacity characteristics determined by FEM analyses

5.1. Numerical analyses simulating model tests

5.1.1. Program code and calculation conditions

To examine the more detailed characteristics of the bearing capacity under seepage, numerical analyses were conducted using the finite element method (FEM). The FEM code GeoFem, developed by the Port and Airport Research Institute (PARI) (Kobayashi, 1988), was used in this study. Since the initial development of the code, when an elasto-plastic model

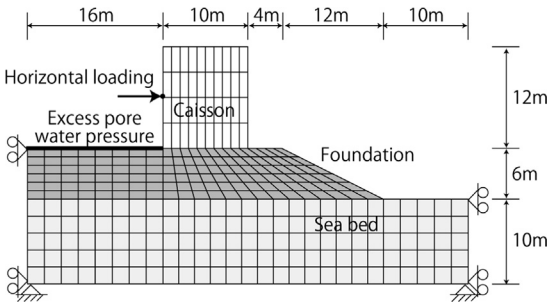

Fig. 22. Finite element mesh modelling commonly-used breakwaters.

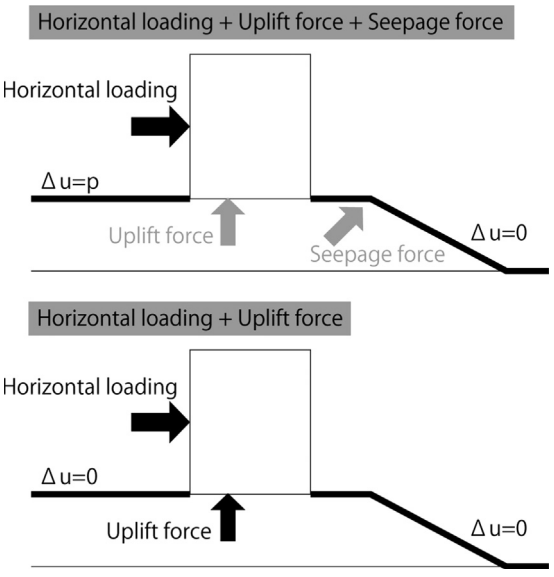

Fig. 23. Conceptual diagram of forces in calculation.

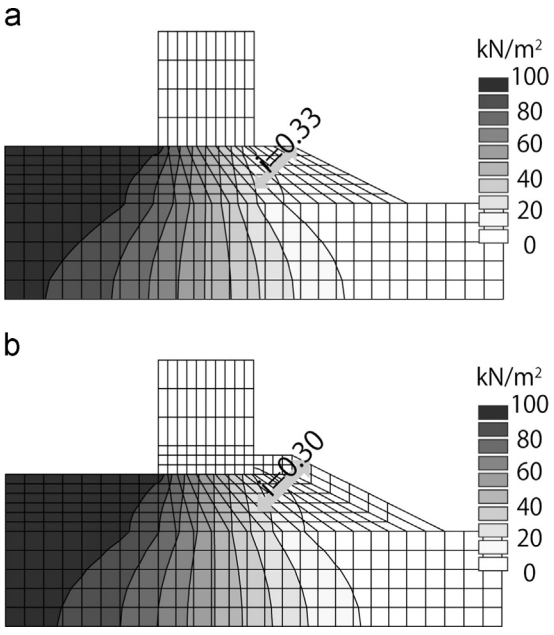

Fig. 24. Distribution of excess pore water pressure in commonly-used breakwaters models. (a) No counter embankment, (b) counter embankment.

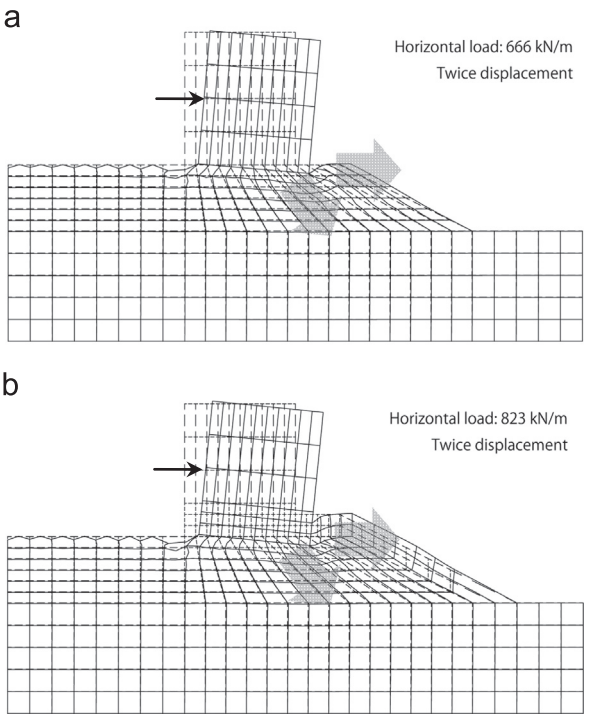

Fig. 25. Deformation behaviour of commonly-used breakwaters models, (a) no counter embankment, (b) counter embankment.

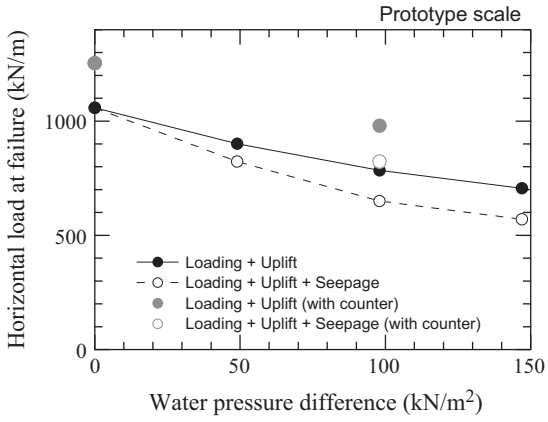

Fig. 26. Relationship between water pressure difference and horizontal load at bearing capacity.

that complied with the Mohr–Coulomb criterion was used, improvements have been made to add constitutive laws, such as the modified Cam-Clay model and Sekiguchi and Ohta (1977). In this study, however, an elasto-plastic model that complies with the Mohr–Coulomb criterion was selected because it has been the most commonly used to simulate the ground behaviour of a rubble foundation. This code enables the analysis of the ground behaviour as failure approaches using a hypothetical elasto-viscoplastic algorithm (Zienkiewicz and Cormeau, 1974).

Fig. 18 shows the element mesh used for the calculations, which model the virtual models A and B used for the model tests. An elasto-plastic model that complies with the Mohr–Coulomb criterion and an elastic model were used to model the

rubble foundation and other components, as indicated in Table 3. The table also gives two shear strengths for the rubble foundation, namely, the strength that includes a hypothetical adhesion of 20 kN/m^2 and that without adhesion. The design standard for port and airport facilities in Japan (OCDI, 2009) prescribes that the hypothetical adhesion should be taken into account because Kobayashi et al. (1987) showed the applicability of a circular slip analysis using hypothetical adhesion to the simulation of some devastated grounds. The shear strength of a rubble foundation significantly depends on the confining pressure, and Kobayashi et al. (1987) incorporated the hypothetical adhesion into the shear strength as a calculation technique for considering the dependency. However, the seepage force may decrease the confined pressure of the rubble foundation, and using the hypothetical adhesion would lead to an overestimation of the shear strength of the foundation. Therefore, calculations without adhesion were also conducted.

The present FEM code assumed a linear relationship between mean flow velocity $\bar{v}$ and hydraulic gradient i of the rubble foundation, in conformance with Darcy's law. The code enables the coupling of the ground deformation with the excess pore water pressure using Biot's theory (1941). This theory utilizes a simultaneous equation obtained from the equilibrium and continuity equations for the coupling. As Darcy's law is used in the continuity equation of Biot's theory, the relationship between v and i is linearised. Although the relationship is actually non-linear, as mentioned earlier, a linear relationship was used to avoid a complicated calculation procedure. Regarding the loading method, the nodal point of the caisson was horizontally loaded under seepage, and the loading was stopped when the foundation collapsed.

5.1.2. Results of numerical analyses of model tests

Fig. 19 shows the calculated excess pore water pressure. The water pressure at the bottom of the rubble foundation of virtual model B (Fig. 19(a)) was found to be almost the same as that measured in the model test (see Fig. 15(a)). Hydraulic gradient i, around the top of the slope, was about 0.1. In contrast, the i of virtual model A (Fig. 19(b)) was about 0.4, which is similar to the value obtained by the model tests (see Fig. 15(b)). Furthermore, the distributions of excess pore water pressure obtained by the calculation and the model tests were similar.

Although several cases were conducted to examine the bearing capacity, the deformation behaviours determined by the calculation were almost the same. As an example, the deformation diagram for the case with no adhesion, with seepage, and using virtual model A is shown in Fig. 20. The illustrated displacement was doubled to make the deformation more visible. As shown in the figure, the laterally and downward deformed area occurred under the corner of the caisson, which caused the top of the slope to move forward. This behaviour was similar to that of Case BC12 in Fig. 14, which confirmed that the FEM analyses could be used to simulate the fundamental deformation observed in the model tests.

Fig. 21 shows the relationship between the load and the displacement at the nodal point of the caisson. In virtual model B (Fig. 21(a)), the seepage force slightly decreased the bearing capacity regardless of the rubble foundation adhesion, and ground failure did not occur. The loaded model ground used for the test did not collapse with seepage either. Meanwhile, the bearing capacity of virtual model B, shown in Fig. 21(b), was reduced by the seepage force to 16 and 33% with and without adhesion, respectively. According to the model test results, the bearing capacity decreased by approximately 23–36%. This rate of reduction is similar to that of one of the cases without adhesion. Consequently, the numerical analyses without consideration of the hypothetical adhesion were found to accurately simulate the model tests.

5.2. Numerical analyses simulating breakwaters commonly used in field

5.2.1. Program code and calculation conditions

In this section, we describe other FEM analyses that were used to confirm the reduction effect of seepage on the bearing capacity of breakwaters commonly used in the field. Hydraulic gradient i in the profile was considered to be in the horizontal direction under the caisson, which is different from that in the model tests. The direction of i under a caisson could somewhat affect the bearing capacity. The effect of the counterweight embankment, which was used to reinforce the bearing capacity, was also examined.

As in the above, the applied FEM code was GeoFem, and the calculation conditions were also nearly the same. Based on the previous FEM results, shear strength c was set to 0 kN/m^2 and ϕ to 45°, without considering the hypothetical adhesion in the foundation. The unit weight of the caisson was 14.7 kN/m^3, taking the buoyancy force into account.

Fig. 22 shows the element mesh used for the calculations. In one case, a counterweight of thickness of 2 m was used to investigate the effect of a counterweight on the bearing capacity. To generate a range in excess pore water pressure on the surface of the rubble foundation in front of the caisson, the nodal point of the caisson was horizontally loaded under seepage. However, the excess pore water pressure also produced an uplift force that acted on the caisson. The uplift force reduced the overburden pressure on the caisson, and consequently, decreased the confined pressure and bearing capacity of the rubble foundation. Since the main purpose of this study was to assess the effect of seepage on the bearing capacity, a force corresponding to the uplift force was added in the case without seepage, as shown in Fig. 23. This enabled the direct comparison of the calculation cases, thereby enabling the determination of the specific effect of seepage.

5.2.2. Results of numerical analyses of commonly used breakwaters

Fig. 24 shows the distribution of the excess pore water pressure for a water pressure difference of 98 kN/m^2, which corresponds to a water level difference of 10 m. The values for hydraulic gradient i around the top of the slope, for the cases

with and without a counterweight embankment, were about 0.33 and 0.30, respectively. It was found that a counterweight with a thickness of 2 m could not significantly reduce i.

Two representative deformation diagrams of the cases subjected to a water pressure difference of 98 kN/m^2 are shown in Fig. 25, where the displacement is doubled. In these cases, the laterally and downward deformed area also occurred under the corner of the caisson, which caused the top of the slope to move forward. This behaviour was not affected by the counterweight.

The relationship between the water pressure difference and the horizontal load at the beginning of the limit state of the bearing capacity is shown in Fig. 26. The results for the case without the counterweight shows that the bearing capacity gradually decreased with the increasing water pressure difference. The uplift force, due to a difference of 98 kN/m^2, reduced the bearing capacity by 26%. The seepage force also decreased the bearing capacity, and this force, due to a difference of 98 kN/m^2, for example, weakened the rubble foundation by 17%. Thus, the effect of seepage force cannot be disregarded when estimating the bearing capacity, and it should be considered in the design of breakwaters. Dong et al. (2012) and Zen et al. (2013) found that the seepage reduced the bearing capacity by about 50%. However, this reduction included the effect of the uplift force and the seepage force, and the bearing capacity was assessed based on the amount of settlement of a caisson, and not the ground strength. The specific reduction due to the seepage force is considered to be lower.

Fig. 26 also includes the calculated data for cases with the counterweight embankment, which shows a significant increase in the bearing capacity, even for a thickness of 2 m, with and without seepage. If we consider that an i of 0.33 caused a 17% reduction in the bearing capacity, a slight change in i, from 0.33 to 0.30, produced by adding a counterweight embankment, would have a little effect on the bearing capacity. It could be said that the overburden pressure produced by the counterweight substantially increased the bearing capacity.

6. Summary and conclusions

In the present study, centrifuge model tests and FEM analyses have been used to examine the stability of a breakwater foundation and the characteristics of the bearing capacity under seepage produced by a tsunami-induced water level difference. The results of the experiments are summarized below.

(1) The results of the centrifuge model tests revealed that the seabed under a rubble foundation was gradually scoured below the front bottom corner of a caisson due to the occurrence of seepage flow at the foundation. A series of tests, based on the similarity rule of seepage, was conducted to determine whether boiling and piping occurred in the rubble foundation. The results of these tests, in turn, revealed that light boiling occurred only in the foundations with a high hydraulic gradient; the boiling was not significantly developed. This boiling pattern is consistent with theory. It must be noted that foundation scouring by overflow is beyond the scope of this paper, although it potentially encourages boiling and/or piping. As the next step of this study, it will be important to examine the effect of foundation scouring brought about by overflow.

(2) The bearing capacity of a rubble foundation with seepage was also examined by centrifuge model tests. To focus on the specific effect of seepage, the lateral water pressure and the uplift force that act on a caisson were eliminated from the model tests. It was observed that the actual seepage force could break down the rubble foundation under an inclined load. It had also first been confirmed by the model tests that the seepage force reduced the bearing capacity of the foundation. Here, it must be noted that seepage from the bottom in the model tests could cause a greater reduction in the bearing capacity.

(3) The results of the simulation of the model tests by FEM analyses confirmed that the analyses could be used to reproduce the bearing capacity characteristics observed in the model tests. A series of FEM analyses was also used to simulate the profiles of commonly used breakwaters. The results of these analyses showed that the bearing capacity decreased with seepage, even in commonly used breakwaters. The reduction was 17% for a water pressure difference of 98 kN/m^2, which corresponds to a difference in water level of 10 m; this should be taken into account in the design of breakwaters. In addition, the overburden pressure generated by a counterweight embankment was found to significantly increase the bearing capacity.

Acknowledgments

The authors wish to thank several organizations. Firstly, we would like to thank the Ports and Harbours Bureau of the Ministry of Transport of Japan for their financial support of our study. Next, we would like to thank the Port and Airport Department of the Tohoku Regional Development Bureau of the Ministry of Transport of Japan for the provision of their measurements of the Kamaishi breakwaters.

Appendix A. Similarity rule of seepage in rubble rocks in centrifuge

Appendix A explains the similarity rule of the seepage in a rubble foundation during centrifugal acceleration. There is a clear correlation between mean velocity $\bar{v}$ and hydraulic gradient i of the seepage flow, and i can be expressed as the sum of the viscous and inertial terms as follows:

$$i = a\bar{v} + b\bar{v}^2 \tag{1}$$

Based on the Dupuit–Forchheimer equations, coefficients a and b are assumed to be as follows:

$$a = \alpha_0 \frac{\nu}{g} \frac{(1-n)^3}{n^2 {d_{15}}^2} \tag{2a}$$

Table A1
Similarity ratio of seepage.

		Prototype	Model (gravitational)	Model (centrifugal)			
Fundamental conditions	Centrifugal acceleration, g	1	1	N	N	N	N
	General dimension, H	1	$1/N$	$1/N$	$1/N$	$1/N$	$1/N$
	Soil particle diameter, D	1	$1/N$	$1/N$	$1/N$	1	1
	Dynamic viscosity, ν	1	1	1	N	1	N
Water pressure	Water pressure u/stress, σ	1	$1/N$	1	1	1	1
Ground stress	Hydraulic gradient, i	1	1	1	1	1	1
Laminar flow	Coefficient, a	1	N^2	N	N^2	$1/N$	1
	Mean flow velocity, $\bar{v}$	1	$1/N^2$	$1/N$	$1/N^2$	N	1
	Time of seepage, t	1	N	1	N	$1/N^2$	$1/N$
	Reynolds number, R_e	1	$1/N^3$	$1/N^2$	$1/N^4$	N	$1/N$
Turbulent flow	Coefficient, b	1	N	1	1	$1/N$	$1/N$
	Mean flow velocity, $\bar{v}$	1	$1/\sqrt{N}$	1	1	$\sqrt{N}$	$\sqrt{N}$
	Time of seepage, t	1	$1/\sqrt{N}$	$1/N$	$1/N$	$1/N^{3/2}$	$1/N^{3/2}$
	Reynolds number, R_e	1	$1/N^{3/2}$	$1/N$	$1/N^2$	$\sqrt{N}$	$1/\sqrt{N}$

Note: Ratios in grey cells were used in the study.

$$b = \beta_0 \frac{1}{g} \frac{1-n}{n^3 d_{15}} \tag{2b}$$

here, α_0 and β_0 are the introduced coefficients, ν is the dynamic coefficient of the viscosity of water, n is the porosity of the ground, d_{15} is the 15% grain size, and g is the gravitational acceleration. Assuming that the hydrostatic pressure is balanced, Eq. (1) can be transformed into the following equations using excess pore water pressure Δu:

$$i_x = \frac{1}{\gamma_w} \frac{\partial \Delta u}{\partial x} = a_x \bar{v}_x + b_x \bar{v}_x{}^2 \tag{3a}$$

$$i_y = \frac{1}{\gamma_w} \frac{\partial \Delta u}{\partial y} = a_y \bar{v}_y + b_y \bar{v}_y{}^2 \tag{3b}$$

here, x and y denote the x and y directions. The continuity equation can also be shown to be as follows, assuming incompressibility of water and a fully saturated ground:

$$\frac{\partial \bar{v}_x}{\partial x} + \frac{\partial \bar{v}_y}{\partial y} = 0 \tag{4}$$

The two-dimensional distribution of Δu is given by Eqs. (3a), (3b) and (4). Meanwhile, the seepage force per unit volume is given by $i\gamma_w$ (where γ_w is the unit weight of water), which can produce piping and/or boiling and reduce the bearing capacity. Therefore, the actual Δu used to determine i must be accurately obtained, even for model tests, satisfying the simultaneous Eqs. (3a), (3b) and (4).

If the seepage is a laminar flow with low velocity or small grain size, Darcy's law would hold because it is dominated by the first terms on the right-hand side of Eqs. (3a) and (3b), which represent the viscous property. In this case, simultaneous Eqs. (3a), (3b) and (4) would become the Laplace equations if a had a constant direction and position and the theoretical solution could be obtained. Moreover, the distribution of Δu can be determined regardless of a.

In contrast, seepage in a rubble foundation with a large grain size is a turbulent flow, and is dominated by the second terms on the right-hand side of Eqs. (3a) and (3b), which represent the inertial property. In this case, it is difficult to obtain the theoretical solution using Eqs. (3a), (3b) and (4). However, the distribution of Δu can also be determined regardless of b if b has a constant direction and position. This means that the model tests can be used to reproduce the actual distribution of Δu if the seepage flow is turbulent. Therefore, before the seepage model tests are conducted, it is necessary to determine whether the flow is turbulent, in which case i is proportional to the square of $\bar{v}$. The determination is discussed in Appendix B.

According to Eqs. (1), (2a) and (2b), the similarity law of seepage can be expressed as in Table A1, where parameter N represents the geometric rate on a prototype scale. The table includes the laws of the similarity between the model tests conducted in a gravitational field and the centrifugal tests for different soil particle sizes and/or viscosities of water. Moreover, the Reynolds's numbers that determine the characteristics of the water flow in a void are also shown in the table. In the present centrifuge model tests, $1/N$-scale crushed stones were used as the rubble foundation and water as the void fluid. As mentioned previously, the inertia term is dominant owing to the turbulent flow of the seepage. Therefore, the similarity laws in the grey area of the table can be adapted for the model tests. For example, the ratios of the mean velocity and time of the seepage in the model tests are 1 and $1/N$, respectively.

Since Reynolds's number is $1/N$ for turbulent flow, the water flow in a void would not be strictly reproduced in these centrifuge model tests. However, it is difficult in practice to simultaneously satisfy both Eq. (1) and the Reynolds's number because this would require the dynamic coefficient of viscosity to be $1/N$ times that of water, or for the particle size of the crushed stones to be $1/N^{1/3}$ times that of one prototype-scale rock. In the present study, allowance was made for a change in the Reynolds's number considering that the main purpose of the model tests was to reproduce the distributions of the pore water pressure and the seepage flow velocity by satisfying Eq. (1), and not Reynolds's number. Although this compromise

Table B1
List of test cases for verification of turbulent flow.

Case	Profile	Rock used (g)	Centrifugal acceleration (g)
KM03	Kamaishi port	A	18.75
KM01		0.011–0.58	37.5
KM02			75
OM06	Omaezaki port	B	12.5
OM05		0.50–3.51	25
OM07			50

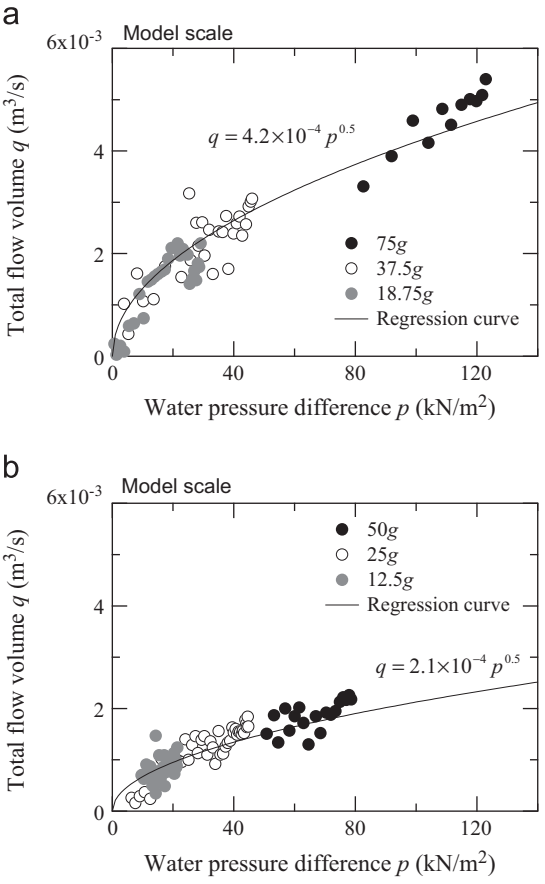

Fig. B1. Relationship between total flow volume and water pressure difference, (a) Kamaishi model (Rock A), (b) Omaezaki model (Rock B).

would reduce the turbulence of the water flow in a void, the seepage force acting on the rubble foundation would be equivalent between the model and the prototype.

Appendix B. Verification of turbulent flow in a rubble foundation

As mentioned in Appendix A, the proportionality between hydraulic gradient i and the square of mean velocity $\bar{v}$, which represents the turbulent seepage flow in a rubble foundation, should be confirmed. Appendix B presents the experimental proof obtained by the centrifuge model tests. The profiles of these tests were the same as those used for the seepage model tests in the main text in the examination of the stability of a rubble foundation. The profiles modelled the Kamaishi and Omaezaki breakwaters, which are shown in Fig. 5(a) and (b). Table B1 lists all the model test cases. The crushed stones were also the same as those used for the tests in the main text, namely Rock A and Rock B. In the model tests, it was difficult to directly measure i and $\bar{v}$. Here, the water pressure difference and the total flow volume through the rubble foundation were substituted for these factors. In addition, the data were collected using three different centrifugal accelerations for both profiles.

Fig. B1 shows the relationship between the total flow volume through the rubble foundation and the water pressure difference for all the test cases on a model scale. A sequence of plots was used to produce the data during the process of increasing the water levels. The figures also include the rhizic regression curves obtained by the method of least squares. In both diagrams of Fig. B1, the plots are distributed around the regression curves, and it can be seen that the water pressure differences were proportional to the square of the total flow volume. This confirms that the seepage flows in the foundations of the model tests were turbulent, which is also the case for the prototype-scale foundation.

References

Beek, V.M., van, Bezuijen, A., Zwanenburg, C., 2010. Piping: centrifuge experiments on scaling effects and levee stability. In: Proceedings of International Conference on Physical Modelling in Geotechnics, 183–189.

Bezuijen, A., Steedman, R.S., 2010. Scaling of hydraulic processes. In: Proceedings of International Conference on Physical Modelling in Geotechnics, 93–98.

Biot, M.A., 1941. General theory of three-dimensional consolidation. J. Appl. Phys. 12, 155–164.

Chang, D.S., Zhang, L.M., 2013. Extended internal stability criteria for soils under seepage. Soils Found. 53 (4), 569–583.

Chen, G., Zheng, L., Zhang, Y., Dong, S., Kasugai, Y., Kawakami, T., 2013. Stability analysis of breakwater under seepage flow using DDA. In: Proceedings of the ASME 32nd International Conference on Ocean, Offshore and Arctic Engineering 6 (10) (pp).

Dong, S., Zen, K., Kasama, K., Wang, B., Takesue, A., 2012. Theoretical and experimental study on tsunami induced instability of caisson type composite breakwater. Mem. Faculty Eng. 72 (2), 55–68.

Ergin, A., Balas, C.E., 2006. Damage risk assessment of breakwaters under tsunami attack. Nat. Hazard. 39 (2), 231–243.

Fujikura, Y., Kokusho, T., 2001. Influences of soil particle gradation on seepage failure and permeability in sand and gravel. J. Jpn. Soc. Civil Eng. 687/III-56, 27–36 (in Japanese).

Fujima, K., 2006. Effect of a submerged bay-mouth breakwater on tsunami behavior analyzed by 2D/3D hybrid model simulation. Nat. Hazard. 39 (2), 179–193.

Hall, S.A., 2006. A methodology for 7D warping and deformation monitoring using time-lapse seismic data. Geophysics 71 (4), O21–O31.

ICE: Coastal structures and breakwaters, ICE, 1994.

Ikari, H., Gotoh, H., Yodoshi, H., 2011. Fundamental study on large deformation analysis of composite breakwater by improved elastoplastic MPS method. J. Jpn. Soc. Civil Eng., Ser. B2 (Coast. Eng.) 67 (2), I_731–I_735 (in Japanese).

Imase, T., Maeda, K., Miyake, M., Sawada, Y., Sumida, H., Tsurugasaki, K., 2012. Destabilization of a caisson-type breakwater by scouring and seepage failure of the seabed due to a tsunami. In: Proceedings of International Conference on Scour and Erosion, 128–135.

Imase, T., Maeda, K., Miyake, M., Tsurugasaki, K., Sawada, Y., Sumida, H., 2011. Instability of caisson-type breakwater due to seepage of tsunami into rubble mound and seabed. J. Jpn. Soc. Civil Eng., Ser. B2 (Coast. Eng.) 67 (2), I_551–I555 (in Japanese).

Irtem, E., Seyfioglu, E., Kabdasli, S., 2011. Experimental investigation on the effects of submerged breakwaters on tsunami run-up height. J. Coast. Res., SI 64, 516–520.

Kazama, M., Noda, T., 2012. Damage statistics (Summary of the 2011 off the Pacific Coast of Tohoku Earthquake damage). Soils Found. 52 (5), 780–792.

Kitazume, M., Miyajima, S., 1995. Development of PHRI Mark II geotechnical centrifuge. Technical Note of the Port and Harbour Research Institute No. 812, 1–35.

Kobayashi, M., 1988. Stability analysis of geotechnical structures by adaptive finite element procedure. Report of the Port and Harbour Research Institute 27 (2), 3–22.

Kobayashi, M., Terashi, M., Takahashi, K., 1987. Bearing capacity of a rubble mound supporting a gravity structure. Report of the Port and Harbour Research Institute 26 (5), 215–252.

Lin, P., Karunarathna, S.A., 2007. Numerical study of solitary wave interaction with porous breakwaters. J. Waterw. Port Coastal Ocean Eng. 133 (5), 352–363.

Miyake, M., Sumida, H., Maeda, K., Sakai, H., Imase, T., 2009. Development of centrifuge modelling for tsunami and its application to stability of a caisson type breakwater. Annu. J. Civil Eng. Ocean 25, 87–92 (in Japanese).

OCDI - Overseas Coastal Area Development Institute of Japan: Technical Standards and Commentaries for Port and Harbour Facilities in Japan, OCDI, pp. 600–601, 2009.

PIANC: State-of-the-art of Designing and Constructing Berm Breakwaters, PIANC, 2003.

Sassa, S., Sekiguchi, H., 1999. Wave-induced liquefaction of beds of sand in a centrifuge. Geotechnique 49 (5), 621–638.

Sekiguchi, H., Kita, K., Okamoto, O., 1995. Response of poro-elastoplastic beds to standing waves. Soils Found. 35 (3), 31–42.

Sekiguchi, H., Ohta, H., 1977. Induced anisotropy and time dependency in clays, Specialty Session 9. In: Ninth Proceedings of International Conference on Soil Mechanics and Foundation Engineering (ICSMFE), 229–238.

Takahashi, H., Ogawa, K., Hayano, K., Morikawa, Y., Ninomiya, Y., 2010. Centrifuge model test on wave force resistance of artificial seashore reclaimed by granular treated soil. Annu. J. Civil Eng. Ocean 26, 687–692 (in Japanese).

Wang, Q.S., Chen, Z.Y., Jin, Y., Liang, J.H., 2010. Development of a circulating system for water supply in centrifuge model tests. In: Proceedings of International Conference on Physical Modelling in Geotechnics, 285–289.

Zen, K., Kasama, K., Kasugai, Y., Dong, S., 2013. Failure of rubble mound beneath caisson due to earthquake-induced tsunami. In: Proceedings of the ASME 32nd International Conference on Ocean, Offshore and Arctic Engineering 6 (8).

Zienkiewicz, O.C., Cormeau, I.C., 1974. Visco-plasticity and creep in elastic solids, a unified numerical solution approach. Int. J. Numer. Methods Eng. 8, 821–845.